Available online at www.sciencedirect.com
ScienceDirect
Trans. Nonferrous Met. Soc. China 25(2015) 2361−2366
Transactions of Nonferrous Metals Society of China
www.tnmsc.cn

Simulation of pre-precipitation in $Ni_{75}Al_{14}Mo_{11}$ alloy by microscopic phase-field model

Jing-jing LIANG, Rui-qin LI, Yao-Hong ZHAO

School of Mechanical and Power Engineering, North University of China, Taiyuan 030051, China

Received 8 January 2015; accepted 10 June 2015

Abstract: The early precipitation process of $Ni_{75}Al_{14}Mo_{11}$ alloy was simulated by microscopic phase-field model at different temperatures. The microstructure of the alloy, the precipitation time of $L1_0$ structure and occupation probability of the three kinds of atoms were investigated. It is indicated that the non-stoichiometric $L1_0$(I/II) phases are found in the precipitation process. With the temperature increasing, the appearance time of $L1_0$ is brought forward. The $L1_0$(II) structure always precipitates earlier than the $L1_0$(I) structure. Compared with lower temperature, higher temperature brings the formation time of $L1_0$ phase forward and makes $L1_0$ phase have a higher order degree. But lower temperature shortens the process time of the $L1_0$ phase to the $L1_2$ phase. Al and Mo atoms tend to occupy γ site, Ni atom tends to occupy α and β sites. At the same temperature, Al atom has stronger occupation ability than Mo atom in the same site. Ni, Al and Mo collectively form the composited $L1_2$ structure.

Key words: $Ni_{75}Al_{14}Mo_{11}$ alloy; microscopic phase-field model; precipitation incubation period; $L1_0$(I/II) phase

1 Introduction

γ' phase which has the $L1_2$ phase is the main strengthening phase of Ni-based alloys, the existence of which endows the Ni-based alloys with excellent properties at high temperatures. In $Ni_{75}Al_{14}Mo_{11}$ alloy, the $L1_2$ structure is a highly symmetric face-centered cubic lattice, the Ni atoms occupy the eight corner points in the face-centered cubic lattice and the Al atoms occupy the face-centered points [1,2]. Phase-field simulation has been widely used to investigate the phenomenon in material science. For instance, CHEN et al [3] used phase-field modeling to study α phase transformation in Ti−Al−V alloy, and found that the results agreed well with the DICTRA simulations. YAMANAKA et al [4] simulated the microstructural formation and deformation behavior of ferrite-pearlite. They found that it could predict the formation and morphological change of α phase in the Fe−C alloy during the $\gamma\rightarrow\alpha$ transformation. KOYAMA [5] utilized the phase-field modeling to demonstrate the microstructure changes in magnetic materials, such as Ni_2MnGa ferromagnetic shape memory alloy, Fe−Pt nanogranular thin film, Co−Sm−Cu rare-earth magnet, and Fe−Cr−Co spinodal magnet [5]. Phase-field model is also used in nucleation and grain growth [6−9], bimodal particle size distribution [10], rafting [11], precipitation [12] and coarsening [13]. Some researches have been done [14−20] in Ni−Al−X (X=metallic element) alloys. Few works about Ni−Al−Mo alloy have been performed so far [12].

In the pre-precipitation process, atoms diffusion appears in the $L1_2$ phase. Therefore, a variety of transient phases could appear in this process. The main purpose of this work is to find the transitional phase in the early stage of γ' precipitation and the relationship between temperature and transitional phase.

2 Theoretical model

In the phase-field model, all phases or domains in the matrix are characterized by field variables, compositions and order parameters. These field variables are continuous across the interface regions. Microscopic phase-field model based on the diffusion equations which are the discrete lattice forms of the Cahn−Hilliard equation is firstly proposed by KHACHATURYAN [21] and developed by PODURI and CHEN [22,23] for the binary and ternary real alloy systems. Equations of

Foundation item: Project (51275486) supported by the National Natural Science Foundation of China
Corresponding author: Rui-qin LI; Tel: +86-13835113159; E-mail: liruiqin@nuc.edu.cn
DOI: 10.1016/S1003-6326(15)63851-1

ternary alloy systems are

$$\begin{cases}\dfrac{\mathrm{d}P_A(r,t)}{\mathrm{d}t}=\\ \quad\dfrac{1}{k_{\mathrm{B}}T}\sum_{r'}\left[L_{AA}(r-r')\dfrac{\partial F}{\partial P_A(r',t)}+L_{AB}(r-r')\dfrac{\partial F}{\partial P_B(r',t)}\right]+\\ \quad\xi(r,t)\\ \dfrac{\mathrm{d}P_B(r,t)}{\mathrm{d}t}=\\ \quad\dfrac{1}{k_{\mathrm{B}}T}\sum_{r'}\left[L_{BA}(r-r')\dfrac{\partial F}{\partial P_A(r',t)}+L_{BB}(r-r')\dfrac{\partial F}{\partial P_B(r',t)}\right]+\\ \quad\xi(r,t)\end{cases} \tag{1}$$

where $L_{\alpha\beta}(r-r')(\alpha,\ \beta=A,\ B$ or $C)$ is a constant which expresses the exchange probabilities between a pair of atoms, α and β, at lattice sites r and r' per unit time, F is the free energy, T is the temperature, k_{B} is the Boltzamann constant, $\xi(r,\ t)$ is the thermal nose which is assumed to be Gaussian-distributed with average value of zero, t is the aging time, $P_A(r,\ t)$, $P_B(r,\ t)$ and $P_C(r,\ t)$ stand for atom (A, B, C) occupation probabilities at a given lattice site r and a given time t. In ternary alloy systems, $P_A(r,\ t)+P_B(r,\ t)+P_C(r,\ t)=1$, and the free energy F can be approximately expressed by the mean-field theory as

$$\begin{aligned}F=&-\frac{1}{2}\sum_r\sum_{r'}[V_{AB}(r-r')P_A(r)P_B(r')+\\ &V_{BC}(r-r')P_B(r)P_C(r')+V_{AC}(r-r')P_A(r)P_C(r')]+\\ &k_{\mathrm{B}}T\sum_r[P_A(r)\ln(P_A(r))+P_B(r)\ln(P_B(r))+\\ &P_C(r)\ln(P_C(r))]\end{aligned} \tag{2}$$

where $V_{\alpha\beta}(r-r')$ expresses the effective exchange interaction energy between α and β ($\alpha,\ \beta=A,\ B,\ C$), which contains chemical interaction energy $V_{\alpha\beta}(r-r')_{\mathrm{ch}}$ and elastic energy $V_{\alpha\beta}(r-r')_{\mathrm{el}}$ [24]:

$$V_{\alpha\beta}(r-r')=V_{\alpha\beta}(r-r')_{\mathrm{ch}}+V_{\alpha\beta}(r-r')_{\mathrm{el}} \tag{3}$$

Using four-neighbor atoms interaction energy is more precise in describing $V_{\alpha\beta}(r-r')$ than two-neighbor atoms interaction energy for three ternary alloys.

In the reciprocal space, $V_{\alpha\beta}(r-r')$ is expressed as

$$\begin{aligned}V_{\alpha\beta}(k')=&4V_{\alpha\beta}^1[\cos(2\pi h')\cdot\cos(2\pi k')+\cos(2\pi h')+\\ &\cos(2\pi k')]+2V_{\alpha\beta}^2[\cos4(\pi h')+\cos(4\pi k')+1]+\\ &8V_{\alpha\beta}^3[\cos(4\pi h')\cdot\cos(2\pi k')+\\ &\cos(2\pi h')\cdot\cos(4\pi k')+\cos(2\pi h')\cdot\cos(2\pi k')]+\\ &4V_{\alpha\beta}^4[\cos(4\pi h')\cdot\cos(4\pi k')+\\ &\cos(4\pi h')+\cos(4\pi k')]\end{aligned} \tag{4}$$

Substituting Eqs. (2), (3) and (4) into Eq. (1), a ternary alloy kinetic Eq. (5) in reciprocal space is given:

$$\begin{cases}\dfrac{\mathrm{d}\widetilde{P}_A(k',t)}{\mathrm{d}t}=\dfrac{\widetilde{L}_{AA}(k')}{k_{\mathrm{B}}T}\Big\{\widetilde{V}_{AC}(k')\widetilde{P}_A(k',t)+\\ \quad\dfrac{1}{2}[-\widetilde{V}_{AB}(k')+\widetilde{V}_{BC}(k')+\widetilde{V}_{AC}(k')]\widetilde{P}_B(k',t)+\\ \quad k_{\mathrm{B}}T\left[\ln\dfrac{P_A(r,t)}{1-P_A(r,t)-P_B(r,t)}\right]_{k'}\Big\}+\\ \quad\dfrac{\widetilde{L}_{AB}(k')}{k_{\mathrm{B}}T}\Big\{\widetilde{V}_{BC}(k')\widetilde{P}_B(k',t)+\\ \quad\dfrac{1}{2}[-\widetilde{V}_{AB}(k')+\widetilde{V}_{BC}(k')+\widetilde{V}_{AC}(k')]\widetilde{P}_A(k',t)+\\ \quad k_{\mathrm{B}}T\left[\ln\dfrac{P_B(r,t)}{1-P_A(r,t)-P_B(r,t)}\right]_{k'}\Big\}+\xi(k',t)\\ \dfrac{\mathrm{d}\widetilde{P}_B(k',t)}{\mathrm{d}t}=\dfrac{\widetilde{L}_{BA}(k')}{k_{\mathrm{B}}T}\Big\{\widetilde{V}_{AC}(k')\widetilde{P}_A(k',t)+\\ \quad\dfrac{1}{2}[-\widetilde{V}_{AB}(k')+\widetilde{V}_{BC}(k')+\widetilde{V}_{AC}(k')]P_B(k',t)+\\ \quad k_{\mathrm{B}}T\left[\ln\dfrac{P_A(r,t)}{1-P_A(r,t)-P_B(r,t)}\right]_{k'}\Big\}+\\ \quad\dfrac{\widetilde{L}_{BB}(k')}{k_{\mathrm{B}}T}\Big\{\widetilde{V}_{BC}(k')\widetilde{P}_B(k',t)+\\ \quad\dfrac{1}{2}[-\widetilde{V}_{AB}(k')+\widetilde{V}_{BC}(k')+\widetilde{V}_{AC}(k')]\widetilde{P}_A(k',t)+\\ \quad k_{\mathrm{B}}T\left[\ln\dfrac{P_B(r,t)}{1-P_A(r,t)-P_B(r,t)}\right]_{k'}\Big\}+\xi(k',t)\end{cases} \tag{5}$$

where

$$\left[\ln\frac{P_A(r,t)}{1-P_A(r,t)-P_B(r,t)}\right]_{k'},\left[\ln\frac{P_B(r,t)}{1-P_A(r,t)-P_B(r,t)}\right]_{k'},$$

$V_{AB}(k)$, $V_{BC}(k)$, and $V_{AC}(k)$ are the Fourier transformations of the corresponding functions in the real space.

3 Simulation results

3.1 Transformation process of $L1_0$ to $L1_2$

Figure 1 indicates the ordered crystal structures of $L1_0$ phase, $L1_2$ phase and their projections along [001] direction. The white ball indicates the Al atom and the black ball indicates the Ni atom. The $L1_0$ phase has two projection styles, the $L1_0$ (II) phase is received by rotating the $L1_0$ (I) structure by 90° along the tetrad-axis in [010] orientation.

Figures 2 and 3 show the microstructure evolution processes at 873 K and 1073 K, respectively. The white grid point expresses the occupation probability of Al atom, the lighter the white color is, the greater the probability is.

From Figs. 2 and 3, we can observe that the $L1_0$ (II)

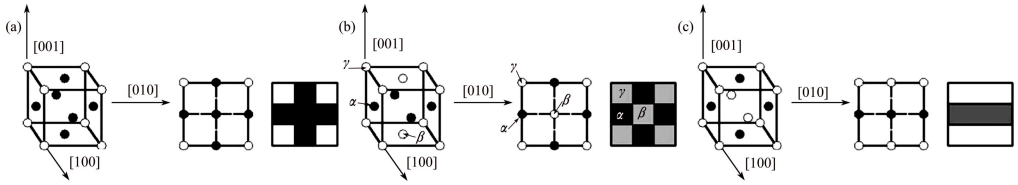

Fig. 1 2D structure projections along [001] of projection images of 3D order structure and its typical image in atomic evolution figure: (a) $L1_2$ phase; (b) $L1_0$ (I) phase; (c) $L1_0$ (II) phase

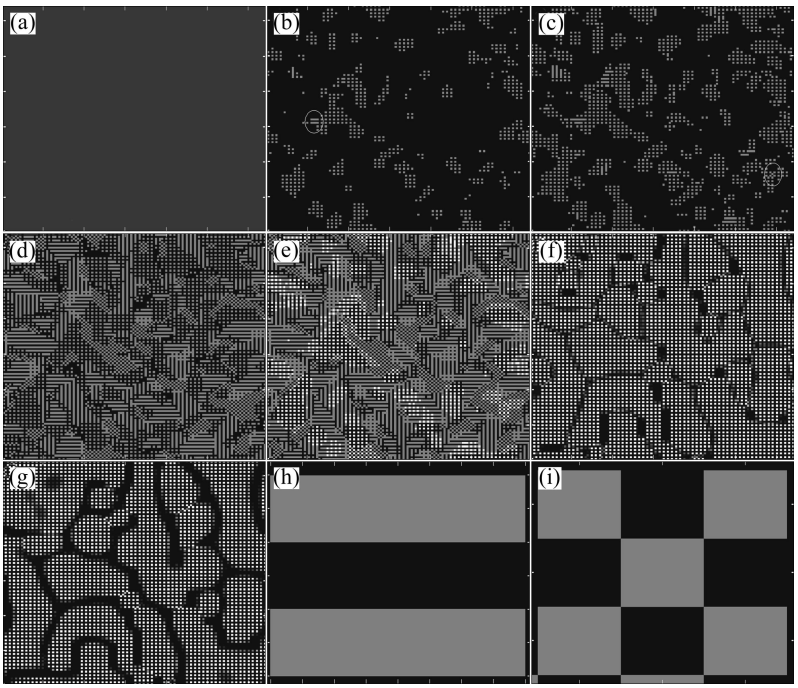

Fig. 2 Microstructure evolution of $Ni_{75}Al_{14}Mo_{11}$ at 873 K: (a) t=5600; (b) t=8700; (c) t=9500; (d) t=14000; (e) t=18700; (f) t=100000; (g) t=200000; (h) Enlargement of white circle in (b); (i) Enlargement of white circle in (c)

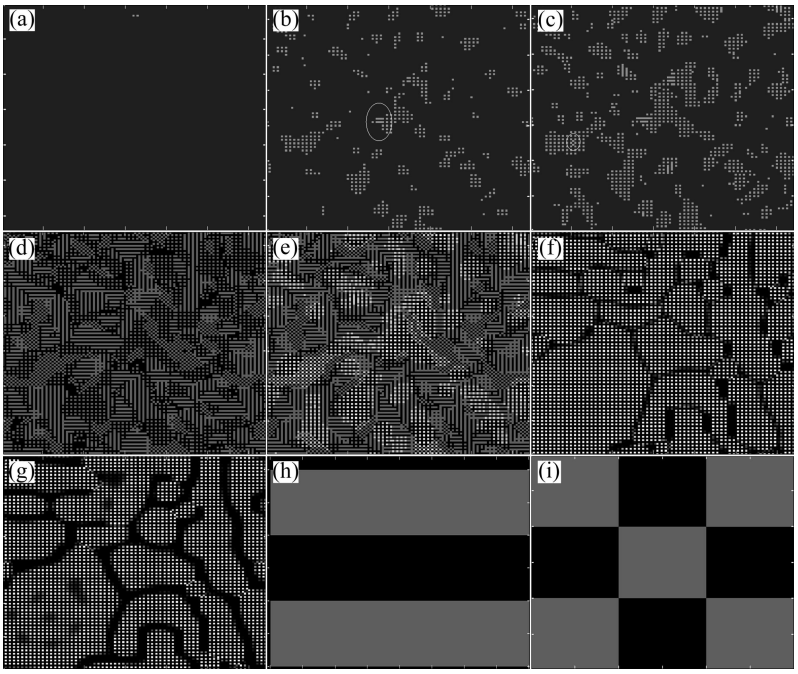

Fig. 3 Microstructure evolution of $Ni_{75}Al_{14}Mo_{11}$ at 1073 K: (a) t=5600; (b) t=8700; (c) t=9500; (d) t=14000; (e) t=18700; (f) t=100000; (g) t=200000; (h) Enlargement of white circle in (b); (i) Enlargement of white circle in (c)

phase (Fig. 2(b) and Fig. 3(b), the enlargements in the white circle are shown Fig. 2(h) and Fig. 3(h)) precipitates earlier (t=8700) from the disordered matrix than the $L1_0$(I) structure (Fig. 2(c) and Fig. 3(c), the enlargements in the white circles are shown in Fig. 2(i) and Fig. 3(i), t=9500) at 873 K or 1073 K. Ahead of this step, in the disordered matrix, the atoms cluster firstly at t=5600, then the short-range ordered phase appears, along with aging proceeding (t=8700−16100), the $L1_0$ and $L1_2$ phases appear. At last, a majority of $L1_0$ structure transforms into $L1_2$ phase and a portion of it disappears.

Figures 2 and 3 are at the same steps, but the white grid points in Fig. 2 are lighter than those in Fig. 3. This shows that the phase in Fig. 2 has higher ordering extent at 1073 K.

3.2 Effect of temperature on precipitation of $L1_0$ phase

In order to investigate the effect of temperature on the $L1_0$ precipitation, five temperatures were chosen to observe the effect on the aging of $Ni_{75}Al_{14}Mo_{11}$ alloy. From Fig. 4, we can observe that as the temperature increases, the precipitation reveals regularity. The structure firstly precipitated is the $L1_0$ (II), and the increase of the temperature does not change the precipitation sequence of the $L1_0$ (II) and $L1_0$ (I).

Figure 5 shows the microstructure evolution of the $Ni_{75}Al_{14}Mo_{11}$ alloy. At this time, the $L1_0$ (II) and $L1_0$ (I) reach the maximal volume fraction. Obviously, we can find that the volume fractions of two different projection styles are almost the same under different temperatures. Therefore, the effect of temperature on the $L1_0$ structure's volume fractions of two styles is weak in $Ni_{75}Al_{14}Mo_{11}$ alloy.

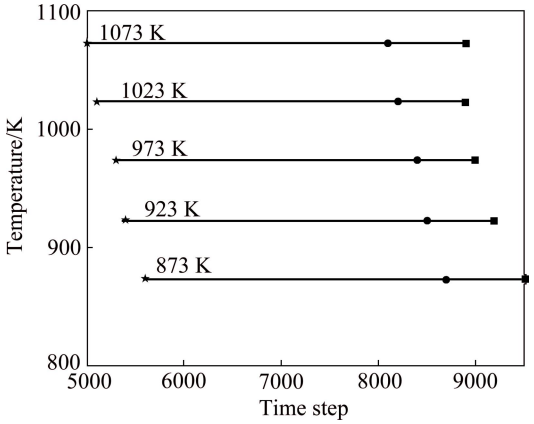

Fig. 4 Effect of temperature on pre-precipitation of $Ni_{75}Al_{14}Mo_{11}$ alloy (★ Indicates the first appearance time of atoms clusters; ● Indicates the first appearance time of $L1_0$(II); ■ Indicates appearance time of $L1_0$(I))

3.3 Occupation probability evolution of Ni, Al and Mo atoms at pre-precipitation stage

From Fig. 6, we can have a further realization about the transformation process of $L1_0$ to $L1_2$. The α, β and γ sites are labeled in Fig. 1. The rise or decline part of the curve indicates the transformation process. At α

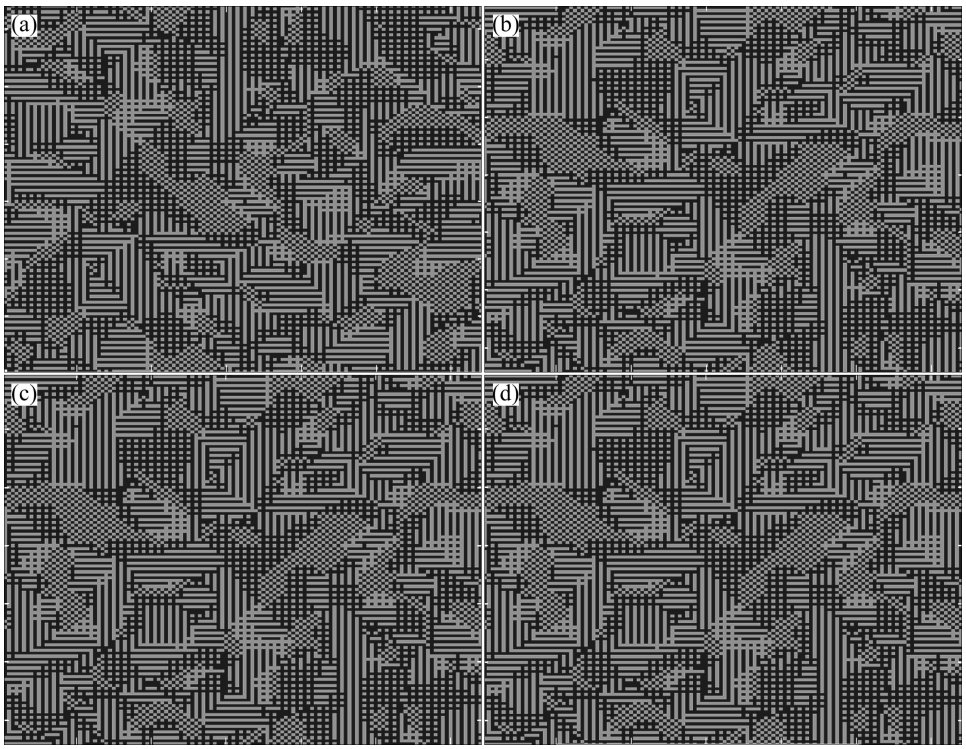

Fig. 5 Microstructure evolution of $Ni_{75}Al_{14}Mo_{11}$ alloy at different temperatures: (a) t=16100, T=873 K; (b) t=16000, T=923 K; (c) t=16000, T=973 K; (d) t=15900, T=1023 K

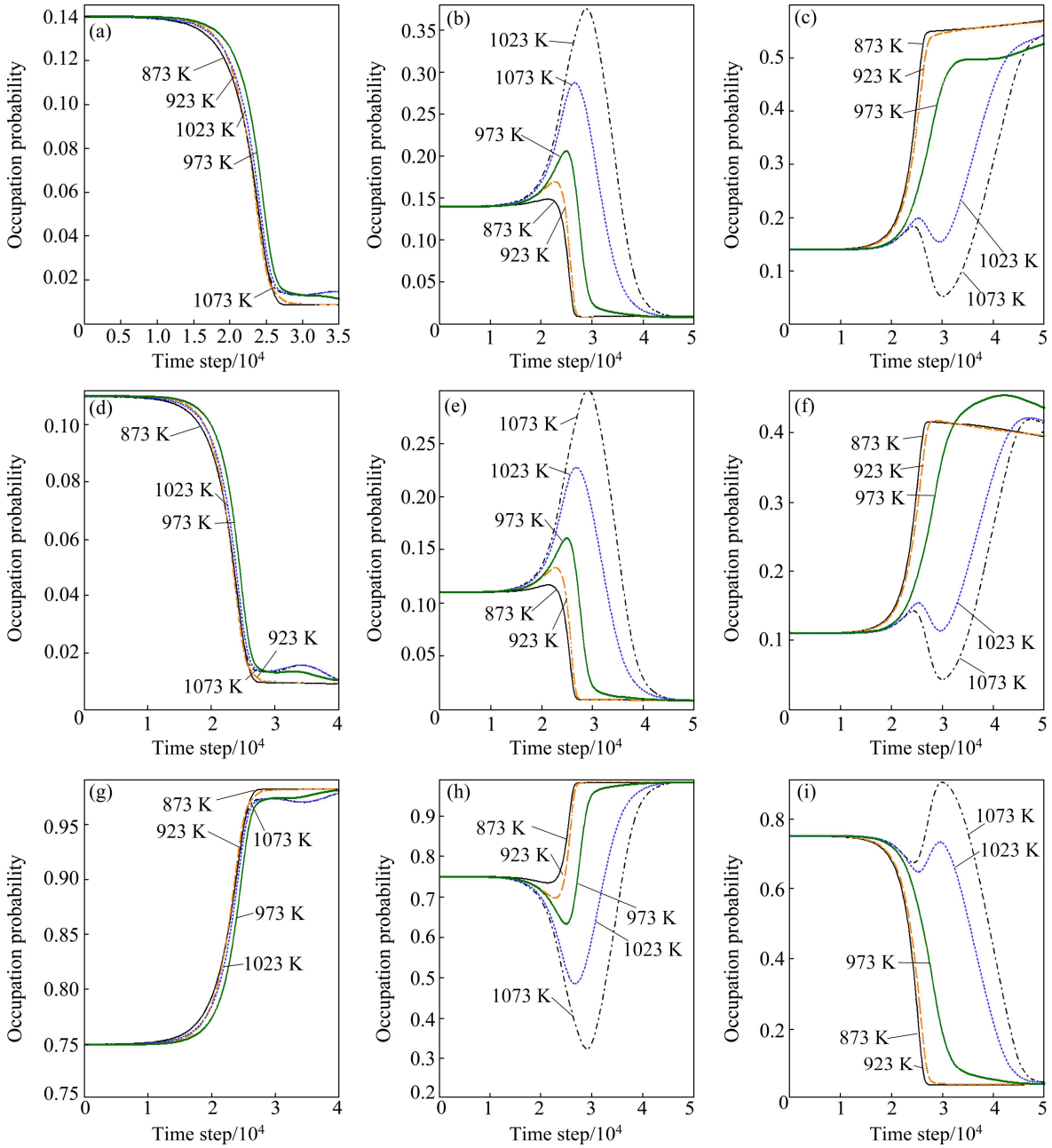

Fig. 6 Atom occupation probability curves of Al (a, b, c), Mo (d, e, f) and Ni (g, h, i) atoms at α (a, d, g), β (b, e, h) and γ (c, f, i) sites

site, Al and Mo atoms firstly undergo balance stage, then the curve starts to descend, but they are chaotic at 873, 923, 1023 and 1073 K. The tardiest transformation occurs at 973 K compared to the other temperatures. At β site, Al atom goes through a transient rising stage, this rise of curve signs the formation of $L1_0$, at a higher temperature, the curve has a distinct rising trend and the time of rise is brought forward (this agrees with Fig. 4), which indicates that at the same time step, the $L1_0$ phase has a better order degree. From Figs. 1(a) and (b), at this time, the occupation probability of Ni atom at the same site should decline accordingly, and it is demonstrated in Fig. 6(h). Along with aging, the curve declines, and the $L1_0$ phase starts to transform to the $L1_2$ phase. Compared with lower temperature, the same transformation at a higher temperature comes up later.

The Mo atom has the similar tendency with the Al atom. The Al atom has a higher number than the Mo atom at the same time step and the same temperature. They tend to occupy the γ site.

4 Conclusions

1) By utilizing the microscopic phase-field model, the aging of $Ni_{75}Al_{14}Mo_{11}$ alloy was simulated at 873, 923, 973, 1023 and 1073 K, and it is found that the $L1_0$ phase precipitates with $L1_0$(I) and $L1_0$(II) two projection styles.

2) The temperature does not change the precipitation sequence of $L1_0$(I) and $L1_0$(II). The $L1_0$(II)

structure always precipitates earlier than the $L1_0$ (I) structure. Temperature has little effect on the volume fractions of $L1_0$ (I) and $L1_0$ (II). Compared with lower temperature, higher temperature brings the formation time of $L1_0$ phase forward and makes $L1_0$ phase have a higher order degree. But lower temperature shortens the process time of the $L1_0$ phase to the $L1_2$ phase.

3) Al and Mo atoms tend to occupy the γ site, Ni atom tends to occupy α and β sites. At the same temperature, Al atom has stronger occupation ability than Mo atom in the same site. Ni, Al and Mo collectively form the composited $L1_2$ phase.

References

[1] ZAPOLSKY H, PAREIGE C, MARTEAU L, BLAVETTE D. Atom probe analyses and numerical calculation of ternary phase in Ni−Al−V system [J]. Calphad, 2001, 25(1): 125−134.

[2] ZHU J Z, LIU Z K, VAITHYANATHAN V, CHEN L Q. Linking phase-field model to CALPHAS: Application to precipitate shape evolution in Ni-base alloys [J]. Scripta Mater, 2002, 46: 401−416.

[3] CHEN Qing, MA Ning, WU Kai-sheng, WANG Yun-zhi. Quantitative phase field modeling of diffusion-controlled precipitate growth and dissolution in Ti−Al−V [J]. Scripta Materialia, 2004, 50: 471−476.

[4] YAMANAKA A, TAKAKI T, TOMITA Y. Elastoplastic phase-field simulation of self-and plastic accommodations in cubic→ tetragonal martensitic transformation [J]. Materials Science and Engineering A, 2008, 480(1−2): 244−252.

[5] KOYAMA T. Phase-field modeling of microstructure evolutions in magnetic materials [J]. Sci Technol Adv Mater, 2008, 9: 1−9.

[6] LUO W, SHEN C, WANG Y. Nucleation of ordered particles at dislocations and formation of split patterns [J]. Acta Mater, 2007, 55: 2579−2586.

[7] ZHANG W, JIN Y, KHACHATURYAN A. Phase field microelasticity modeling of heterogeneous nucleation and growth in martensitic alloy [J]. Acta Mater, 2007, 55: 565−574.

[8] SIMMONS J, WEN Y, SHEN C, WANG Y. Microstructural development involving nucleation and growth phenomena simulated with the phase field method [J]. Mat Sci Eng A, 2004, 365: 136−143.

[9] GRANASY L, BORZSONYI T, PUSZTAI T. Crystal nucleation and growth in binary phase-field theory [J]. Phys Rev Lett, 2002, 88: 206105.

[10] WEN Y, SIMMONS J, SHEN C, WOODWARD C, WANG Y. Phase-field modeling of bimodal particle size distributions during continuous cooling [J]. Acta Mater, 2003, 51: 1123−1132.

[11] ZHOU N, SHEN C, Mills M, WANG Y. Phase field modeling of channel dislocation activity and γ' rafting in single crystal Ni−Al [J]. Acta Mater, 2007, 55: 5369−5381.

[12] WANG Tao, SHENG Guang, LIU Zi-kui, CHEN Long-qing. Coarsening kinetics of γ' precipitates in the Ni−Al−Mo system [J]. Acta Mater, 2008, 56: 5544−5551.

[13] BOISSE J, LECOQ N, PATTE R, ZAPOLSKY H. Phase-field simulation of coarsening of γ precipitates in an ordered γ' matrix [J]. Acta Mater, 2007, 55: 6151−6158.

[14] PODURI R, CHEN L Q. Computer simulation of morphological evolution and coarsening kinetics of δ' (Al_3Li) precipitates in Al−Li alloys [J]. Acta Mater, 1998, 46(5): 1719−1729.

[15] ZHAO Yan, CHEN Zhen, LU Yan-li, ZHANG Li-peng. Microscopic phase-field study on aging behavior of $Ni_{75}Al_{17}Zn_8$ alloy [J]. Transactions of Nonferrous Metals Society of China, 2010, 20(4): 675−681.

[16] CHEN Zheng. Phase-field study on competition precipitation process of Ni−Al−V alloy [J]. Transactions of Nonferrous Metals Society of China, 2015, 25(2): 544−551.

[17] ZHANG Ming-yi, CHEN Zheng, WANG Yong-xin, MA Guang, LU YAN-li, FAN Xiao-li. Effect of atomic structure on migration characteristic and solute segregation of ordered domain interfaces formed in $Ni_{75}Al_xV_{25-x}$ [J]. Transactions of Nonferrous Metals Society of China, 2011, 21(3): 604−611.

[18] YANG Kun, CHEN Zheng, WANG Yong-xin, FAN Xiao-li. Microscopic phase-field study on directional coarsening mechanism caused by interaction between precipitates in Ni−Al−V alloy [J]. Transactions of Nonferrous Metals Society of China, 2013, 23(1): 193−200.

[19] ZHANG Ming-yi, CHEN Zheng, WANG Yong-xin, LU Yan-li, ZHANG Li-peng, ZHAO Yan. Microscopic phase-field simulation of ordered domain interfaces formed between DO22 phases along [100] direction [J]. Transactions of Nonferrous Metals Society of China, 2009, 19(3): 686−693.

[20] HOU Hua, ZHAO Yu-hui, NIU Xiao-feng. 3D anisotropy simulation of dendrites growth with phase field method [J]. Transactions of Nonferrous Metals Society of China, 2008, 18(2): 223−228.

[21] KHACHATURYAN A G. Theory of structural transformations in solids [M]. New York: Wiley, 1983: 23.

[22] PODURI R, CHEN L Q. Computer simulation of morphological evolution and coarsening kinetics of δ' (Al_3Li) precipitates in Al−Li alloys [J]. Acta Mater, 1998, 46(11): 3915−3924.

[23] PODURI R, CHEN L Q. Computer simulation of atomic ordering and compositional clustering in the pseudobinary Ni_3Al−Ni_3V system [J]. Acta Mater, 1998, 46(5): 1719−1729.

$Ni_{75}Al_{14}Mo_{11}$ 合金早期沉淀过程的微观相场法模拟

梁晶晶， 李瑞琴，赵耀红

中北大学 机械与动力工程学院， 太原 030051

摘 要：采用微观相场动力学模型研究不同温度下 $Ni_{75}Al_{14}Mo_{11}$ 合金的早期沉淀过程, 研究合金的微观结构、$L1_0$ 相的析出时间以及 3 种原子的占位概率。结果表明：沉淀过程中析出 $L1_0$ 非化学计量比有序相，$L1_0$ 相有 I 型和 II 型 2 种结构，随着温度的增加，$L1_0$ 相析出的时间提前。在沉淀的过程，II 型 $L1_0$ 结构的析出时间比 I 型 $L1_0$ 结构的析出时间早。温度升高缩短了 $L1_0$ 相的形成时间，使 $L1_0$ 相有序度更高；温度越低，$L1_0$ 相向 $L1_2$ 相的转变时间越短。Al 原子和 Mo 原子占据 γ 位， Ni 原子占据 α 位和 β 位，在同样的温度和格点下，Al 原子的占位几率大于 Mo 原子的占位几率。Ni、Al 和 Mo 3 种原子构成复合 $L1_2$ 相。

关键词：$Ni_{75}Al_{14}Mo_{11}$ 合金；微观相场模型；沉淀孕育期；$L1_0$ (I/II) 相

(Edited by Yun-bin HE)